




Coherent longitudinal acoustic phonon dynamics in antimony sulfide under hydrostatic pressureBowen Guan ¹, Ruiqi Wu,¹ Fuxiang Ma,¹ Runxing Hao ¹, Xinzhao Wu,² Yuanfei Jiang,¹ Mingxing Jin,^{1,*} and Qingyi Li ^{1,†}¹*Institute of Atomic and Molecular Physics, Jilin Provincial Key Laboratory of Applied Atomic and Molecular Spectroscopy, Jilin University, Changchun 130012, People's Republic of China*²*Institute of Theoretical Chemistry, College of Chemistry, Jilin University, Changchun 130023, People's Republic of China*

(Received 16 March 2024; revised 30 April 2024; accepted 28 May 2024; published 5 June 2024)

Van der Waals (vdW) solids, composed of ultrathin atomic layers with weak interlayer bonding, possess unique electronic and thermal properties and exhibit sensitivity to external stimuli such as compressive strain. Understanding and manipulation of their thermal transport behavior through strain engineering is crucial to optimize thermal management and energy conversion, which still remains elusive. Here, we demonstrate pressure manipulation on cross-plane coherent longitudinal acoustic phonon (CLAP) dynamics in bulk antimony sulfide (Sb_2S_3) under hydrostatic pressure through both systematic femtosecond pump-probe spectroscopy and first-principles calculations. The experimental group velocity of CLAP increases monotonically by around 68% upon compression up to 5.06 GPa. First-principles calculations reveal that this dramatic change comes from the modification of phonon dispersion. Our findings shed light on the manipulation of thermal transport and energy conversion via compressive strain, which contribute to the thermal management in device engineering.

DOI: [10.1103/PhysRevB.109.224303](https://doi.org/10.1103/PhysRevB.109.224303)**I. INTRODUCTION**

Recently, van der Waals (vdW) solids have attracted considerable interest and been utilized in electronic, photonic, plasmonic, and numerous device applications [1–5]. Composed of a few atomic layers with weak interlayer bonding, vdW solids exhibit high anisotropy [6,7] and tunable flexibility [8], which hold great promise in stimuli-response devices [9]. To improve the performance of practical devices, optimization on thermal management and energy conversion are always challenging [10], where in-depth understanding and manipulation of the lattice dynamics and thermal transport are urgently needed. Despite this importance, relevant research still remains elusive. In crystalline materials, thermal transport primarily arises from lattice vibrations, or so-called phonons [11,12]. Specifically, compared with optical phonons, acoustic phonons usually exhibit enhanced heat transfer capabilities, making them pivotal for thermal transport [13,14]. Among various manipulation methods, strain is able to effectively tune the phononic properties and thermal transport of vdW solids [15,16]. In this context, investigations on acoustic phonon dynamics together with strain engineering may inspire the optimization of thermal management in actual device designing.

As a typical vdW semiconductor, antimony sulfide (Sb_2S_3) has received an upsurge of attention in the past decade due to its desirable features, such as low cost, nontoxicity, earth abundance, and many other decent photovoltaic and thermoelectric properties [17,18]. Sb_2S_3 , with a band gap of ~ 1.7 – 1.8 eV, is crystallized with an orthorhombic structure

(*Pnma*) consisting of infinite one-dimensional (1D) [Sb_4S_6] ribbons (see Fig. 1), which is structurally appealing and progressively participating in device design [19,20]. In spite of these benefits, experimental studies into its fundamental properties such as lattice dynamics are still deficient. To our knowledge, only a coherent B_{3g} longitudinal optical phonon mode was observed and investigated with pump-probe spectroscopy by Chong *et al.* [21], which is difficult to be applicable to heat conduction in Sb_2S_3 . Therefore, to examine the modification of acoustic phonon dynamics in Sb_2S_3 under the influence of external stimuli such as pressure will not only reveal its intrinsic properties and in turn guide material optimization, but also fine tune its thermal transport to broaden its prospective applications in device engineering.

In this paper, we investigate the cross-plane coherent longitudinal acoustic phonon (CLAP) dynamics in bulk Sb_2S_3 under hydrostatic pressure via femtosecond pump-probe spectroscopy. The cleavage plane (*a-b* plane) is perpendicular to the incident direction of the pump pulse (see Fig. 1). Utilizing a diamond anvil cell (DAC), hydrostatic pressure up to 5.06 GPa was generated. We found that the experimental group velocity of CLAP increases by $\sim 68\%$ with growing pressure. Moreover, at a specific pressure, the interference oscillation frequency is negatively correlated with the wavelength of the probe, whereas it is independent of the pump fluence. Meanwhile, the theoretical group velocity increases monotonically by $\sim 63\%$ in the range of pressure measurement. First-principles calculations suggest that the variation of the experimental group velocity results from an enormously modified phonon dispersion, which leads to significant manipulation of thermal transport in Sb_2S_3 .

*mxjin@jlu.edu.cn

†liqy21@jlu.edu.cn

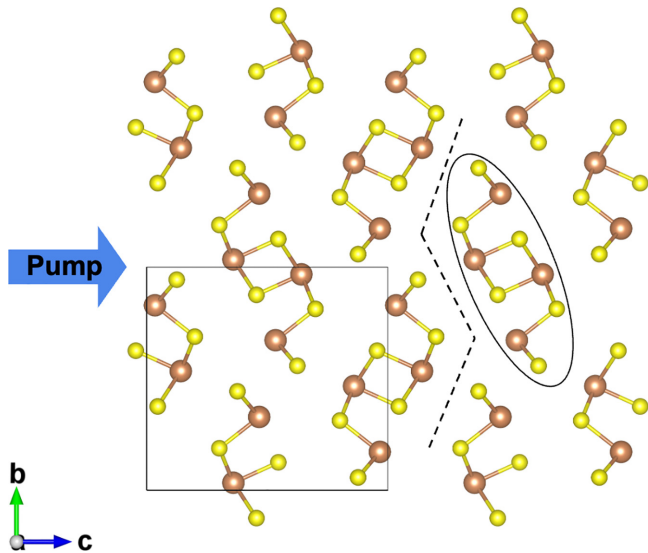


FIG. 1. The crystal structure of Sb_2S_3 from the perspective along the a axis, with the unit cell enclosed by a black square. Brown and yellow balls represent Sb and S atoms, respectively. One $[\text{Sb}_4\text{S}_6]$ ribbon is encircled by an ellipse. The cleavage plane is shown with the black dashed line. The incident direction of the pump pulse is along the c axis.

II. METHODS

A. Experimental setup

In our ultrafast spectroscopy experiments, ultrashort laser pulses (35 fs, 800 nm, 1 kHz) were generated from a regenerative Ti:sapphire femtosecond laser amplifier (Coherent Libra). The 400-nm pump pulse was produced using a barium metaborate (BBO) crystal by frequency doubling, while the supercontinuum probe pulse (450–950 nm) was gained by transmitting the 800-nm fundamental laser pulse through a 3-mm-thick sapphire plate. A motorized translation stage was used to provide a computer-controlled time delay between the pump and the probe pulses. The DAC used for pressurization has an anvil culet of 600 μm diameter, with silicone oil as the pressure-transmitting medium. Similar with our previous experimental system [22], by combining the DAC with broadband femtosecond pump-probe spectroscopy, we can examine the ultrafast transient reflection (TR) spectra of the Sb_2S_3 sample under hydrostatic pressure. We performed mechanical exfoliation with 38-mm blue adhesive plastic film (Ultron Systems) on the original Sb_2S_3 (Sunano, purity > 99.999%) to obtain a surface-flat bulk Sb_2S_3 sample, which is sized to fit the culet of DAC and has a thickness of around 20 μm . All experiments were performed at ambient temperature.

B. First-principles calculations

The structure optimization of bulk Sb_2S_3 under hydrostatic pressure was conducted with density functional theory (DFT) [23] using the Vienna *ab initio* simulation package (VASP, version 6.3.2) [24]. The revised Perdew-Burke-Ernzerhof generalized-gradient approximation (GGA) functional for solids (PBEsol) [25] was used for all calculations. Projector augmented-wave (PAW) pseudopotentials [26] with five

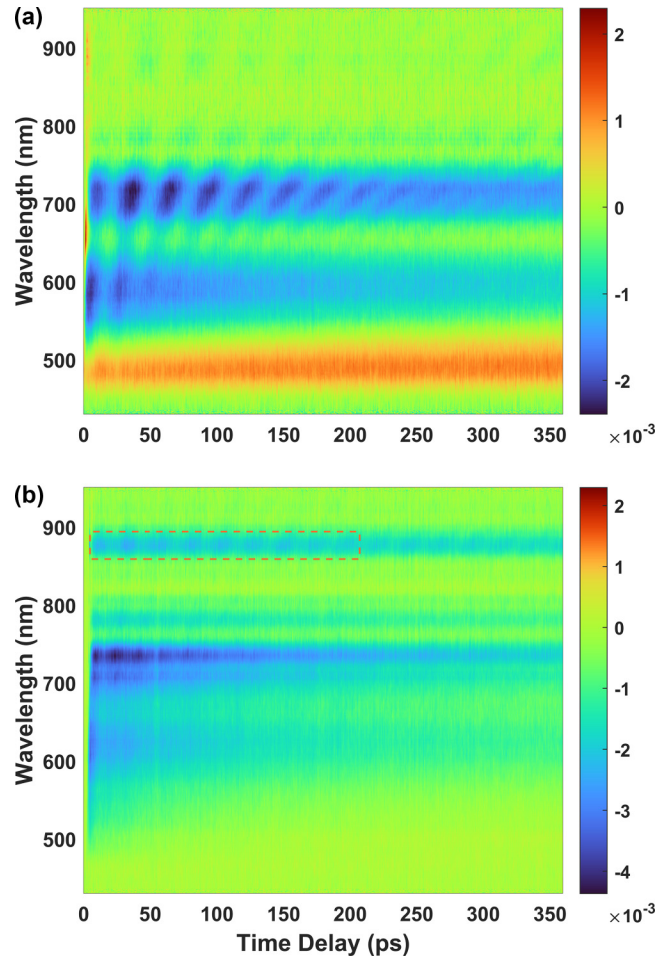


FIG. 2. 2D contour plot of TR spectra of Sb_2S_3 at (a) 1 atm and (b) 5.06 GPa.

valence electrons for Sb ($5s^25p^3$) and six valence electrons for S ($3s^23p^4$) were used to describe the core-valence interaction. Initial lattice constants of Sb_2S_3 are $a = 3.87 \text{ \AA}$, $b = 11.23 \text{ \AA}$, and $c = 12.13 \text{ \AA}$. A plane-wave basis set with a 400 eV cutoff energy was employed to expand wave functions for electrons. The integration over the Brillouin zone was represented using a Monkhorst-Pack [27] $6 \times 2 \times 2$ k -point mesh. The total energy convergence was set to be 1.0×10^{-5} eV/atom, while the force convergence on each atom is below 1.0×10^{-4} eV/ \AA . Hydrostatic pressures from 0 to 5.06 GPa were applied to all lattice constants to investigate the pressure-induced structure relaxation. All phonon dispersions are calculated using the supercell force-constant method [28–30] with a $6 \times 1 \times 3$ supercell containing 360 atoms in the same VASP version. The force-constant matrix is computed with the finite-difference approach. The width of the displacement of each ion is 0.015 \AA and the electronic convergence criterion is 1.0×10^{-8} eV.

III. RESULTS AND DISCUSSION

Figure 2 shows the TR spectra of Sb_2S_3 at ambient pressure and 5.06 GPa, respectively. The x axis represents the delay time between the pump and probe pulse, while the y axis

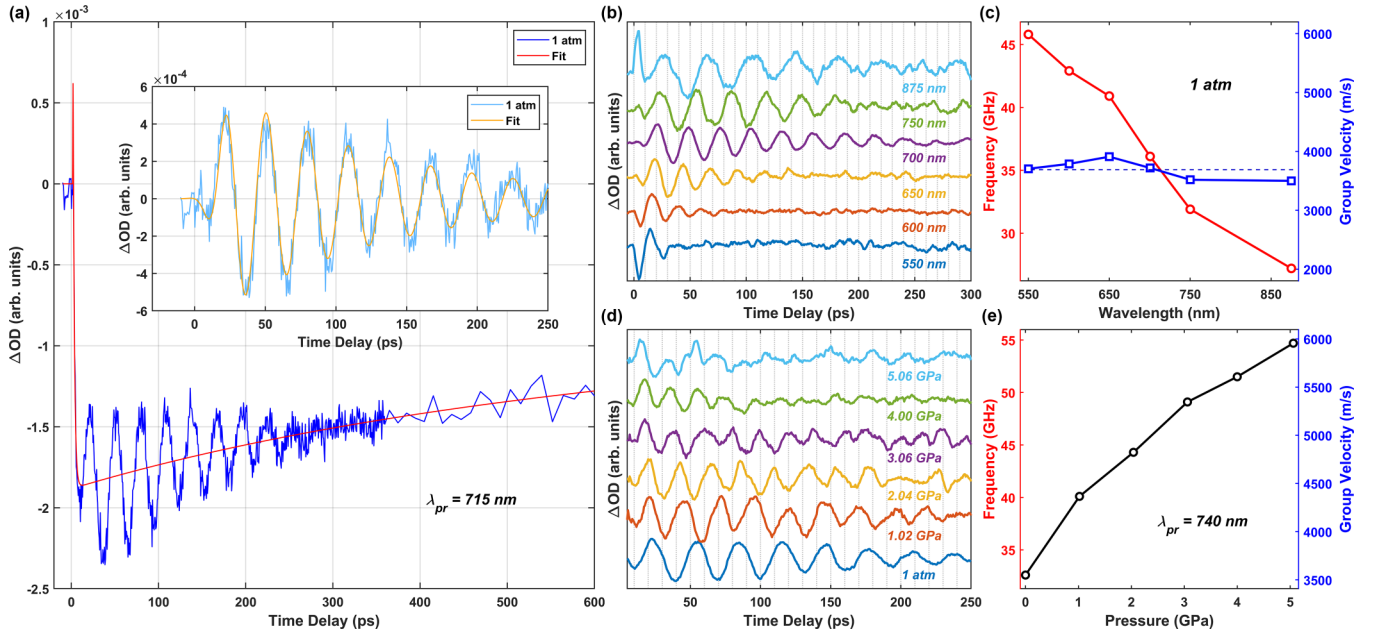


FIG. 3. (a) Typical relaxation curve of Sb_2S_3 (blue line) and electron relaxation dynamics fitting (red line) under ambient pressure. Inset: Coherent acoustic phonon dynamic curve (cyan) and the fitting (orange). The selected probe wavelength is 715 nm. Oscillations are further extracted with (b) different probe wavelengths and (d) pressures. (c) and (e) illustrates the dependence of oscillation frequencies with probe wavelengths and pressures, respectively. The right-hand axis of (c) and (e) represents the derived group velocities of CLAPs from the oscillation frequencies. The blue dashed line in (c) illustrates the average of the derived group velocity of CLAP at 1 atm, namely 3690.2 m/s.

represents the spectral range of the probe. Figure 2(a) exhibits an obvious oscillation structure, which is mainly distributed in ~ 0 –300 ps from the visible to near-IR region. The period of the oscillation is about tens of picoseconds, showing a straightforward feature of coherent acoustic phonons [31,32]. Sb_2S_3 has a high absorption coefficient of $\sim 8 \times 10^4 \text{ cm}^{-1}$ at 400 nm [33]. Thus, the pump light penetration depth is around 125 nm, which is significantly smaller than the sample thickness. Furthermore, as shown in Figs. 2(a) and 3(b), the oscillation period is dependent on the wavelength of the probe. Therefore, we can safely attribute the observed coherent acoustic phonons to propagating wave fronts [34]. When the pressure increases to 5.06 GPa, as shown in Fig. 2(b), the oscillation in the visible region almost disappears, and only what is in the near IR still remains [as shown in the dashed box in Fig. 2(b)]. This may be related to the comprehensive effect of the pressure-induced changes in both the optical penetration depth and the group velocity of the coherent acoustic phonons.

Figure 3(a) illustrates a typical TR signal (blue line) of Sb_2S_3 under ambient pressure. Within the first few picoseconds, the signal has a sudden and rapid response, which originates from the excited charge carriers in the material by the pump. Then the signal begins to relax slowly, accompanied by a damped oscillation that lasts ~ 280 ps with an oscillatory period of ~ 29 ps. In order to obtain pure oscillations, the following function convoluted by a Gaussian instrument response function (IRF) was used to fit the TR signal,

$$\frac{\Delta R}{R} = \sum_{i=1}^n A_i e^{-t/\tau_i} + A_{\text{osc}} e^{-t/\tau_{\text{osc}}} \cos(2\pi f t + \phi), \quad (1)$$

where A_i and τ_i denote the amplitude and lifetime of the i th electron relaxation dynamics, while A_{osc} , τ_{osc} , f , and ϕ denote the amplitude, decay time, frequency, and phase of the oscillations, respectively. By subtracting the electron dynamics [red line in Fig. 3(a)] from the original TR decay curve, clean oscillations can be acquired, as shown in the inset in Fig. 3(a). The orange line stands for the damped oscillation fitting, corresponding to the second term in Eq. (1).

By performing a global fitting on the TR spectra, the wavelength and pressure dependence of the oscillations could be obtained, as depicted in Figs. 3(b) and 3(d), respectively. By further fitting these oscillations with Eq. (1), it can be found in Figs. 3(c) and 3(e) that (i) the oscillation frequency decreases monotonically with the probe wavelength increasing from 550 to 875 nm, and (ii) the oscillation frequency increases almost linearly by $\sim 68\%$ with a slope of $df/dP \sim 4.24 \pm 0.39 \text{ GHz/GPa}$, as the pressure grows from 1 atm to 5.06 GPa. Such oscillations can be attributed to CLAP signals, whose origin was explained first by Thomsen *et al.* and can be understood explicitly with Thomsen's equation [35],

$$f = \frac{2v_s n}{\lambda_{\text{pr}}}, \quad (2)$$

where f and v_s represent the oscillation frequency and the sound velocity or phonon group velocity in the material, n represents the real part of the refractive index, and λ_{pr} denotes the wavelength of the probe. Based on a previous study, the change of the refractive index n in Sb_2S_3 within the pressure range in our experiment is very small, hence we take $n = 3.4$ as a constant [36]. Thereafter, v_s can be derived with Eq. (2), and the results are as shown with the right-hand axes in Figs. 3(c) and 3(e). It is worth noting that when the external pressure is fixed, v_s is supposed to be still and independent of

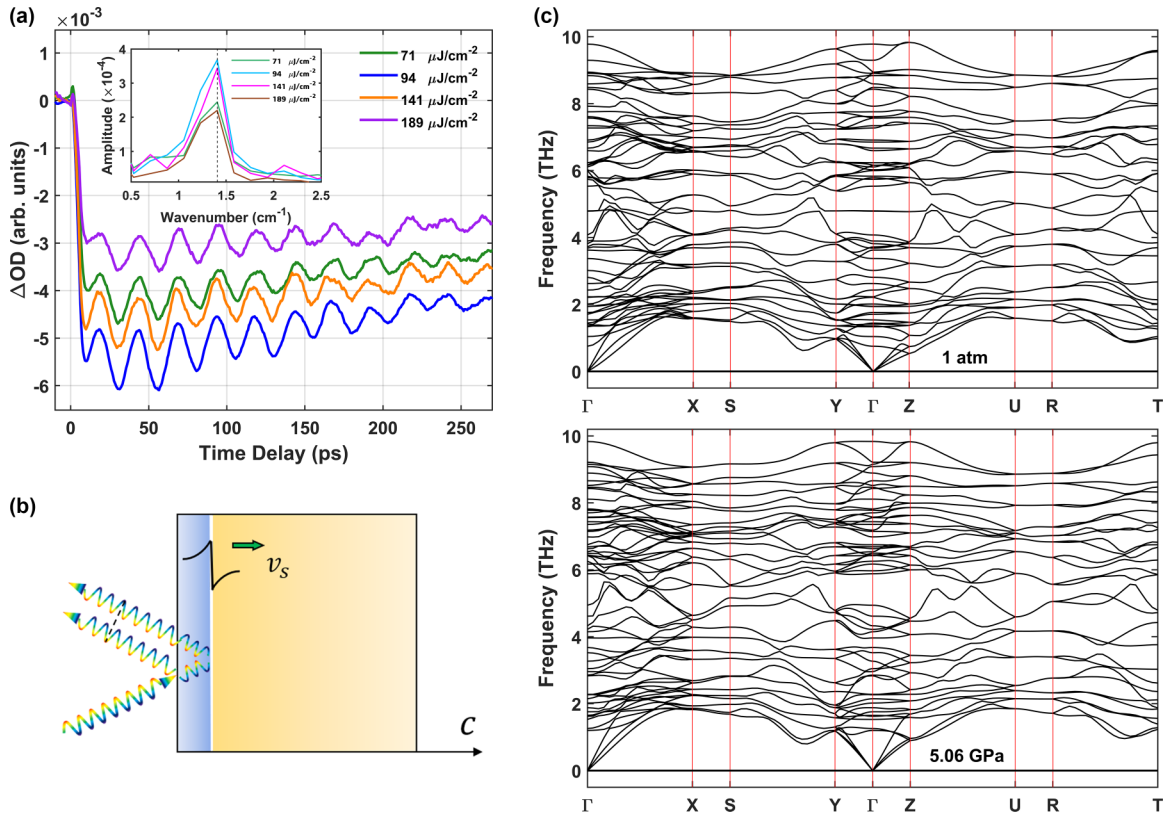


FIG. 4. (a) Comparison of the oscillations under different pump fluences at ambient pressure. The wavelength of the probe is 725 nm. The inset shows the FFT results, in which the oscillations under different pump fluences have the same peak position (1.406 cm^{-1} , i.e., 42.2 GHz). (b) Schematic diagram of the origin of the interference oscillation. The strain pulse is illustrated with the black curve. The blue and orange areas denote parts of the material where the strain pulse traveled and did not travel, respectively. The white line between the blue and orange areas represents the moving interface. (c) First-principles calculations of phonon dispersions for Sb_2S_3 at both 1 atm and 5.06 GPa using the supercell force-constant method in VASP version 6.3.2. The size of the supercell is $6 \times 1 \times 3$, containing 360 atoms. The selected q -point path is $\Gamma \rightarrow X \rightarrow S \rightarrow Y \rightarrow \Gamma \rightarrow Z \rightarrow U \rightarrow R \rightarrow T$, with high-symmetry points $\Gamma = (0, 0, 0)$, $X = (0.5, 0, 0)$, $S = (0.5, 0.5, 0)$, $Y = (0, 0.5, 0)$, $Z = (0, 0, 0.5)$, $U = (0.5, 0, 0.5)$, $R = (0.5, 0.5, 0.5)$, and $T = (0, 0.5, 0.5)$.

λ_{pr} , since it is an intrinsic quantity of the crystal. The derived v_s for different probes and their average are illustrated with the blue line and the blue dashed line separately in Fig. 3(c). The fluctuation of derived v_s , which comes from the fitting inaccuracy and the λ_{pr} -dependent n , is less than 5% for all λ_{pr} . We further explore the variation of the oscillations under different pump fluences at ambient pressure, and the result is shown in Fig. 4(a). It is found that the oscillation frequency is independent of the pump fluence we adopted, which is further confirmed by the fast Fourier transform (FFT) results in the inset.

The main CLAP generation mechanism in semiconductors is based on the deformation potential (DP) theory [35,37], which is responsible for the findings here in Sb_2S_3 [see Fig. 4(b)]. First, the electron-hole pairs are excited by the pump on the material surface, which changes the electronic distribution and in turn the equilibrium position in the lattice. Thereafter, the atomic displacements are generated, creating a strain pulse, i.e., CLAPs. The CLAPs propagate in the material along the cross-plane direction (c axis) with a sound velocity v_s and alter the local dielectric constant, causing the formation of a moving interface. When the probe pulses reach the material, some of them are immediately reflected by the surface, while the rest are transmitted into the material and

reflected by the moving interface. The detected oscillation then comes from the interference between these two sets of reflected probes.

In the preceding parts, we have experimentally investigated and analyzed the pressure-dependent CLAP characteristics and dynamics in Sb_2S_3 . To gain a more comprehensive understanding of CLAP properties, we further conducted first-principles calculations on the phonon dispersion of Sb_2S_3 under pressure, as illustrated in Fig. 5(a). Γ -Y denotes the in-plane direction, while Γ -Z denotes the cross-plane direction, which is parallel to the propagation of the pump pulse. Group velocities are shown by a color gradient, with a warmer color manifesting higher velocities. The complete phonon dispersion at 1 atm and 5.06 GPa, which can be seen in Fig. 4(c), exhibits no imaginary modes, indicating that the optimized structure of Sb_2S_3 is achieved in the range of our pressure measurement. As depicted in Fig. 5(a), the acoustic phonons along the cross-plane direction is low frequency with low velocities at ambient pressure, due to the weak vdW interlayer bonding. Upon compression up to 5.06 GPa, group velocities of the cross-plane phonon modes increase dramatically by a factor of ~ 1.63 , which is in good agreement with the pressure evolution of the experimental group velocities, as shown in Fig. 5(b). Moreover, it can be seen from Fig. 5(a) that the

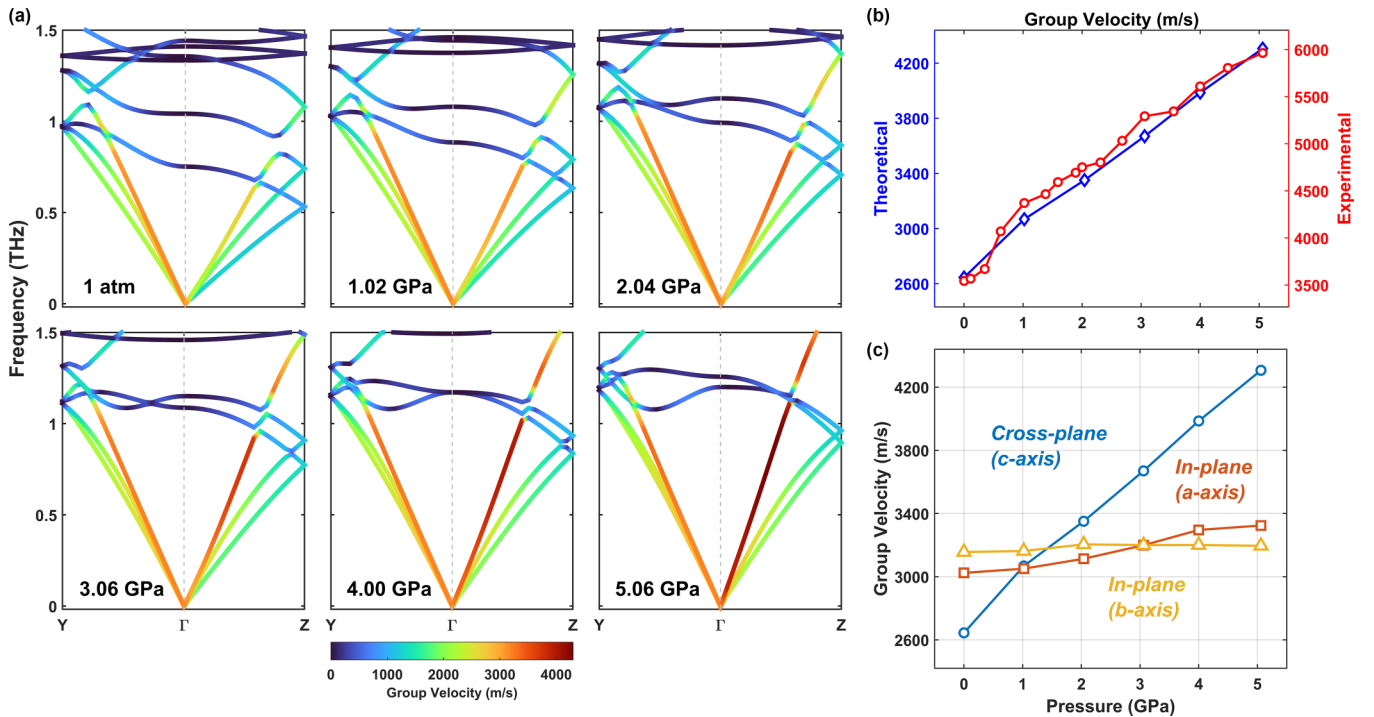


FIG. 5. (a) Pressure evolution of phonon dispersion and phonon group velocity along both in-plane (Γ -Y) and cross-plane (Γ -Z) directions. A color gradient is used to display the slope of the dispersion curve, which is defined as the group velocity of phonons. (b) Theoretical sound velocities (blue line) compared with the derived experimental group velocities of CLAPs (red line) under different pressures. The wavelength of the probe is 740 nm here. (c) Theoretical group velocities of longitudinal acoustic phonons along different directions as a function of pressure.

frequency range of dispersions along the Γ -Z direction becomes wider as the pressure goes up, which may be related to pressure-enhanced phonon-phonon scattering and a reduction in phonon lifetime [7]. In addition, the group velocities of in-plane longitudinal acoustic phonons vary quite slightly under different pressures, compared with that of the cross-plane ones, as shown in Fig. 5(c). Such a result is derived from the anisotropy of Sb_2S_3 , indicating that compressive strain is able to manipulate the cross-plane thermal conductivity more prominently, in contrast with isotropic 3D materials, whose thermal conductivity in all directions can be almost equally and moderately affected by pressure, such as Si [38,39].

IV. CONCLUSION

In summary, we investigated the cross-plane CLAP behavior in bulk Sb_2S_3 under hydrostatic pressure using femtosecond pump-probe spectroscopy. As pressure was elevated from 1 atm to 5.06 GPa, the CLAP group velocity exhibited an increase by a factor of 1.68. First-principles calculations revealed that the cross-plane phonon group velocity increased by a factor of ~ 1.63 with increasing pressure, very

consistent with experimental results. Our calculations indicate that the modified phonon dispersion gives rise to the observed growth of the pressure-induced CLAP group velocity and a possible decrease in phonon lifetime. Basically, a higher phonon group velocity could enhance lattice thermal conductivity, while a decreased phonon lifetime might reduce it. The precise determination of thermal transport modulation under varying pressures remains challenging due to the intricate interplay between these two factors. Nevertheless, our findings shed light on potential predominant mechanisms within Sb_2S_3 that influence thermal transport, offering insights for future thermal management strategies via strain engineering. Finally, our results suggest that femtosecond pump-probe spectroscopy is well suited for the study of lattice dynamics under extreme conditions and can be extended to electronic and phononic studies in related vdW solids.

ACKNOWLEDGMENTS

We acknowledge support from the National Key Research and Development Program (No. 2019YFA0307701), and the National Natural Science Foundation of China (NSFC No. 11974138 and No. 12204191).

- [1] T. Echtermeyer, L. Britnell, P. Jasnós, A. Lombardo, R. Gorbachev, A. Grigorenko, A. Geim, A. Ferrari, and K. Novoselov, *Nat. Commun.* **2**, 458 (2011).
 [2] Y. Liu, H. Zhou, R. Cheng, W. Yu, Y. Huang, and X. Duan, *Nano Lett.* **14**, 1413 (2014).

- [3] T. Yang, B. Zheng, Z. Wang, T. Xu, C. Pan, J. Zou, X. Zhang, Z. Qi, H. Liu, Y. Feng, W. Hu, F. Miao, L. Sun, X. Duan, and A. Pan, *Nat. Commun.* **8**, 1906 (2017).
 [4] F. Withers, O. Del Pozo-Zamudio, A. Mishchenko, A. P. Rooney, A. Gholinia, K. Watanabe, T. Taniguchi, S. J. Haigh,

- A. K. Geim, A. I. Tartakovskii, and K. S. Novoselov, *Nat. Mater.* **14**, 301 (2015).
- [5] W. J. Yu, Y. Liu, H. Zhou, A. Yin, Z. Li, Y. Huang, and X. Duan, *Nat. Nanotechnol.* **8**, 952 (2013).
- [6] A. Alofi and G. P. Srivastava, *Phys. Rev. B* **87**, 115421 (2013).
- [7] X. Meng, T. Pandey, J. Jeong, S. Fu, J. Yang, K. Chen, A. Singh, F. He, X. Xu, J. Zhou, W.-P. Hsieh, A. K. Singh, J.-F. Lin, and Y. Wang, *Phys. Rev. Lett.* **122**, 155901 (2019).
- [8] J. Zhang, Y. Hong, and Y. Yue, *J. Appl. Phys.* **117**, 134307 (2015).
- [9] Y. Gao and B. Xu, *ACS Nano* **12**, 11254 (2018).
- [10] A. L. Moore and L. Shi, *Mater. Today* **17**, 163 (2014).
- [11] Z. Li, D. Shi, J. Yang, W. Luo, C. Wan, and W. Pan, *J. Eur. Ceram. Soc.* **41**, 7981 (2021).
- [12] X. Gu, Y. Wei, X. Yin, B. Li, and R. Yang, *Rev. Mod. Phys.* **90**, 041002 (2018).
- [13] W. Kim, J. Zide, A. Gossard, D. Klenov, S. Stemmer, A. Shakouri, and A. Majumdar, *Phys. Rev. Lett.* **96**, 045901 (2006).
- [14] Y. Zhang, E. Skoug, J. Cain, V. Ozoliņš, D. Morelli, and C. Wolverton, *Phys. Rev. B* **85**, 054306 (2012).
- [15] Z. Ding, Q.-X. Pei, J.-W. Jiang, W. Huang, and Y.-W. Zhang, *Carbon* **96**, 888 (2016).
- [16] H.-K. Mao, X.-J. Chen, Y. Ding, B. Li, and L. Wang, *Rev. Mod. Phys.* **90**, 015007 (2018).
- [17] N. Bansal, F. T. F. O'Mahony, T. Lutz, and S. A. Haque, *Adv. Energy Mater.* **3**, 986 (2013).
- [18] H. Yang, P. Boulet, and M.-C. Record, *Materials* **13**, 4707 (2020).
- [19] Q. Wang, Z. Chen, J. Wang, Y. Xu, Y. Wei, Y. Wei, L. Qiu, H. Lu, Y. Ding, and J. Zhu, *Inorg. Chem. Front.* **6**, 3381 (2019).
- [20] L. Wang, W. Lian, B. Liu, H. Lv, Y. Zhang, X. Wu, T. Wang, J. Gong, T. Chen, and H. Xu, *Adv. Mater.* **34**, 2200723 (2022).
- [21] W. K. Chong, G. Xing, Y. Liu, E. L. Gui, Q. Zhang, Q. Xiong, N. Mathews, C. K. Gan, and T. C. Sum, *Phys. Rev. B* **90**, 035208 (2014).
- [22] Q. Li, L. Sui, G. Niu, J. Jiang, Y. Zhang, L. Che, G. Wu, M. Jin, and K. Yuan, *Phys. Rev. B* **103**, 125416 (2021).
- [23] P. Hohenberg and W. Kohn, *Phys. Rev.* **136**, B864 (1964).
- [24] G. Kresse and J. Furthmüller, *Phys. Rev. B* **54**, 11169 (1996).
- [25] J. P. Perdew, A. Ruzsinszky, G. I. Csonka, O. A. Vydrov, G. E. Scuseria, L. A. Constantin, X. Zhou, and K. Burke, *Phys. Rev. Lett.* **100**, 136406 (2008).
- [26] P. E. Blöchl, *Phys. Rev. B* **50**, 17953 (1994).
- [27] H. J. Monkhorst and J. D. Pack, *Phys. Rev. B* **13**, 5188 (1976).
- [28] G. Kresse, J. Furthmüller, and J. Hafner, *Europhys. Lett.* **32**, 729 (1995).
- [29] K. Parlinski, Z. Q. Li, and Y. Kawazoe, *Phys. Rev. Lett.* **78**, 4063 (1997).
- [30] G. J. Ackland, M. C. Warren, and S. J. Clark, *J. Phys.: Condens. Matter* **9**, 7861 (1997).
- [31] L. Li, F. He, X. Zhao, Z. Tong, and L. Guo, *Phys. Rev. B* **106**, L060304 (2022).
- [32] L. Zhang, Y. Cai, L. Li, W. Feng, R.-T. Wen, S. Shin, and L. Guo, *Photoacoustics* **30**, 100489 (2023).
- [33] R. Kondrotas, C. Chen, and J. Tang, *Joule* **2**, 857 (2018).
- [34] S. Ge, X. Liu, X. Qiao, Q. Wang, Z. Xu, J. Qiu, P.-H. Tan, J. Zhao, and D. Sun, *Sci. Rep.* **4**, 5722 (2014).
- [35] C. Thomsen, H. T. Grahn, H. J. Maris, and J. Tauc, *Phys. Rev. B* **34**, 4129 (1986).
- [36] M. Azadparvar, H. A. R. Aliabad, and E. G. Özdemir, *AIP Adv.* **13**, 065218 (2023).
- [37] P. Ruello and V. E. Gusev, *Ultrasonics* **56**, 21 (2015).
- [38] Y. Zhou, Z.-Y. Dong, W.-P. Hsieh, A. F. Goncharov, and X.-J. Chen, *Nat. Rev. Phys.* **4**, 319 (2022).
- [39] K. D. Parrish, A. Jain, J. M. Larkin, W. A. Saidi, and A. J. H. McGaughey, *Phys. Rev. B* **90**, 235201 (2014).